NASA TECHNICAL NOTE

COMPARISON OF LONGITUDINAL
AERODYNAMIC CHARACTERISTICS
OF CURVED AND STRAIGHT
LEADING-EDGE DELTA WINGS
AT MACH NUMBERS 3 AND 6

by Dewey E. Wornom and Joseph Gera

Langley Research Center
Langley Station, Hampton, Va.

COMPARISON OF LONGITUDINAL AERODYNAMIC CHARACTERISTICS

OF CURVED AND STRAIGHT LEADING-EDGE DELTA WINGS

AT MACH NUMBERS 3 AND 6

By Dewey E. Wornom and Joseph Gera

Langley Research Center
Langley Station, Hampton, Va.

COMPARISON OF LONGITUDINAL AERODYNAMIC CHARACTERISTICS

OF CURVED AND STRAIGHT LEADING-EDGE DELTA WINGS

AT MACH NUMBERS 3 AND 6

By Dewey E. Wornom and Joseph Gera
Langley Research Center

SUMMARY

Force tests have been conducted of three slab-sided delta planform wings, one with a straight leading edge and two with curved leading edges. One curved wing had constant spanwise leading-edge radius and wing thickness and for the other curved wing, the leading-edge radius and wing thickness decreased linearly over the span. The longitudinal characteristics of the three wings were measured over an angle-of-attack range from -5° to approximately 13°. The Reynolds numbers per foot were approximately 2.26 and 0.91×10^6 at Mach numbers of 3 and 6, respectively.

Substantial reductions in drag coefficient with no appreciable difference in lift and pitching-moment characteristics were noted for the curved leading-edge wings as compared with the straight leading-edge wing. At zero-lift conditions the drag coefficients of the curved leading-edge wing with spanwise decreasing leading-edge radius and wing thickness were 26 and 50 percent lower at Mach numbers of 3 and 6, respectively, than that for the straight leading-edge wing. The drag characteristics of the curved leading-edge wing with constant spanwise leading-edge radius and thickness indicated that approximately one-half of the aforementioned zero-lift drag-coefficient reduction resulted from leading-edge curvature, the remaining reduction being due to decreasing leading-edge radius and wing thickness. These reductions in drag coefficient were maintained at lifting conditions and were reflected in maximum lift-drag ratios 16 and 32 percent higher at Mach numbers of 3 and 6, respectively, for the curved leading-edge wing with decreasing spanwise leading-edge radius and wing thickness as compared with the straight leading-edge wing.

INTRODUCTION

Present-day design of fixed straight leading-edge aerodynamic lifting surfaces for flight at moderate or high supersonic speeds are not compatible with low-speed requirements. Highly swept sharp leading edges are required for maximum flight efficiency at supersonic speeds, whereas moderately swept surfaces with rounded leading edges are needed at subsonic speeds. The design problem is further complicated by high-speed aerodynamic heating considerations which

necessitate blunt leading edges that are detrimental to high-speed efficiency. Therefore, the final surface design must be an optimum choice between those required for high- and low-speed flight.

In order to improve further the optimum wing design, consideration was given to altering the geometric aspects of the surface leading edge in view of their effects upon both aerodynamic force and heating characteristics. Experimental results of references 1, 2, and 3 reveal that increasing leading-edge sweep and decreasing leading-edge radius of a straight leading-edge surface improves high-speed flight efficiency. Although such alterations would decrease low-speed flight efficiency, experimental results of reference 4 indicate that introduction of leading-edge curvature would be beneficial. Also, in reference 5, based on the experimental and theoretical results of references 6 and 7, it is shown that the laminar convective heating rate of an aerodynamic leading edge at high speeds is proportional to the cosine of the leading-edge sweep and inversely proportional to the square root of the leading-edge radius. Therefore, in the appendix of this paper an analytical method is presented; this method results in spanwise increasing leading-edge sweep with a corresponding decreasing leading-edge radius, through the introduction of leading-edge curvature, such that the relationship between them that is associated with aerodynamic heating is not altered. Since references 1 and 3 indicate beneficial results by increasing the sweep of a straight leading edge and not by spanwise increasing sweep through leading-edge curvature, the analytical method was applied to a straight leading-edge delta wing, the results of force tests at Mach numbers of 3 and 6 comparing the straight and curved leading-edge wings being presented herein. To isolate the combined effects of spanwise increasing leading-edge sweep and decreasing leading-edge radius, experimental results of the curved leading-edge wing with constant leading-edge radius are also presented.

SYMBOLS

The forces and moments were referred to the stability-axes system whose origin was located at the midpoint of the theoretical wing root chord and in the plane of symmetry. (See fig. 1.)

A,B,C,D
E,F,G,H distances as defined in figure 6

$\bar{c}$ mean geometric chord, in.

C_D drag coefficient, $\dfrac{\text{Drag}}{qS}$

$C_{D,c}$ balance-chamber drag coefficient, $\dfrac{\text{Balance-chamber drag}}{qS}$

$C_{D,o}$ drag coefficient at $C_L = 0$

2

$C_{D,te}$ trailing-edge drag coefficient, $\dfrac{\text{Trailing-edge drag}}{qS}$

C_L lift coefficient, $\dfrac{\text{Lift}}{qS}$

C_m pitching-moment coefficient, $\dfrac{\text{Pitching moment about } 0.5l}{qS\bar{c}}$

d diameter

l length of wing theoretical root chord

L/D lift-drag ratio

M free-stream Mach number

q free-stream dynamic pressure, lb/sq ft

r radius

R leading-edge radius of straight leading-edge wing, in.

R' local leading-edge radius of curved leading-edge wing, in.

S wing reference area, 0.4214 sq ft

t local half-thickness at leading-edge surface (see fig. 6), in.

t_r half-thickness at root of surface (see fig. 6), in.

x,y Cartesian coordinates of curved leading edge (see fig. 1(b), 1(c), or 6), in.

x',y' Cartesian coordinates of origin of leading-edge radii (see fig. 1(c)), in.

α angle of attack, deg

Λ geometric sweep angle of straight leading-edge surface, deg

Λ' local geometric sweep angle of curved leading-edge surface, deg

Λ_e effective sweep angle of straight leading-edge surface (angle between free-stream direction and leading edge), deg

Λ'_e local effective sweep angle of curved leading-edge surface (angle between free-stream direction and leading edge), deg

APPARATUS AND MODELS

The investigation was conducted in the 2-foot hypersonic facility at the Langley Research Center. This facility is of the continuous-flow type and is capable of operating over a Mach number range from 3 to 7. A detailed description of the facility is given in reference 8.

The first curved wing (designated wing II) was designed by applying the analytical method of appendix A to the straight leading-edge wing (designated wing I), whose dimensional details are given in figure 1(a). With a chosen leading-edge sweep angle of $\Lambda' = 79°$ at the wing tip, a semispan of $x = 3.9$ (equal to the semispan of wing I), and an angle of attack of $12°$, the value of $A = 7.80$ was obtained from

$$\tan \Lambda' = -\frac{dy}{dx} = \frac{\sqrt{1 - \cos^2\Lambda_e\left(1 - \frac{x}{A}\right)}}{\sqrt{\cos^2\alpha - 1 + \cos^2\Lambda_e\left(1 - \frac{x}{A}\right)}}$$

Applying the wing-tip boundary conditions of $y = 0$ and $x = 3.9$ yields the value of $B = 18.14$ as obtained from

$$y = \sqrt{\frac{A}{\cos^2\Lambda_e} - A} + x\sqrt{\frac{A\cos^2\alpha}{\cos^2\Lambda_e} - \frac{A}{\cos^2\Lambda_e} + A - x}$$

$$+ \frac{A\cos^2\alpha}{\cos^2\Lambda_e} \sin^{-1} \frac{\sqrt{\frac{A\cos^2\alpha}{\cos^2\Lambda_e} - \frac{A}{\cos^2\Lambda_e} + A - x}}{\sqrt{\frac{A\cos^2\alpha}{\cos^2\Lambda_e}}} + B$$

With the unknown quantities of these equations now determined, the local leading-edge sweep angle Λ' and associated x and y coordinates of the curved leading edge were computed. The coordinates and local sweep angles, together with other dimensional details of wing II, are given in figure 1(b). The leading-edge radius of this wing was held constant so that a comparison between wing II and wing I would reveal only the aerodynamic effects of leading-edge curvature.

The leading-edge curvature of the second curved wing (designated wing III) was determined in the same manner as that stated for wing II. In addition, to obtain the spanwise decreasing leading-edge radius, the following equation was used:

$$R' = \sin \Lambda' - \frac{\dfrac{x - A}{A^2}}{t_r \sqrt{t_r^2 \sin^2 \Lambda' + A^2}} - \frac{t_r \sin \Lambda'}{\sqrt{t_r^2 + \dfrac{A^2}{\sin^2 \Lambda'}}}$$

The resulting values of R' together with other dimensional details of wing III are given in figure 1(c). The wing root half-thickness t_r used was 0.3, which is the root half-thickness of the straight leading-edge wing.

Introduction of curvature to a straight leading-edge wing while the same wing span is maintained results in the curved wing having more wing area than the straight wing. Therefore, to maintain the same aspect ratio of 1.003 for all three wings to give a direct aerodynamic comparison, it was necessary to adjust the trailing edge of wing I until its area was equal to that of the curved wings. This adjustment resulted in the original true delta planform of wing I becoming a clipped delta planform.

Each wing model was mounted in the tunnel test section on a 0.75-inch-diameter sting and a conventional sting-support arrangement.

TESTS, MEASUREMENTS, AND ACCURACY

The wings were tested at angles of attack from -5° to approximately 13°. Other test conditions were as follows:

Mach number	Tunnel stagnation pressure, lb/sq ft	Stagnation temperature, $^\circ$F	Approximate Reynolds number per foot
3.0	2115	95	2.26×10^6
6.0	5570	315	.91

Forces and moments were measured by an electrical strain-gage balance located inside the balance chamber of each wing. The pressures in the balance chamber and along the blunt trailing edge (see fig. 1(a) for orifice locations) were also measured.

The angle-of-attack measurements were corrected for balance and sting deflection under load. The values of angle of attack are estimated to be accurate within $\pm 0.2^\circ$.

Based on the sensitivity of the strain-gage balance, the measured coefficients are accurate within the following limits:

C_L . . . . ±0.005

C_D . . . . ±0.001

C_m . . . . ±0.001

The force data presented herein were not adjusted to free-stream conditions at the base of the wings or balance chamber housing. The estimated accuracy of $C_{D,c}$ and $C_{D,te}$ is ±10 percent of the measured values.

DISCUSSION OF RESULTS

The variation of chamber-pressure and trailing-edge drag coefficient with angle of attack for the three wings tested (wings I, II, and III) is presented in figure 2. The trailing-edge drag coefficient compares favorably with that computed from the theoretical base pressure coefficient based on $1/M^2$. (See table in fig. 2(b).)

The longitudinal aerodynamic characteristics for all three wings are presented in figure 3. Comparison of the lift and pitching-moment coefficients for the three wings shows no appreciable effects on the longitudinal aerodynamic characteristics due to either leading-edge curvature (wing II compared with wing I) or decreasing spanwise leading-edge radius (wing III compared with wing II). The slight decrease in the slope of the pitching-moment curves for wings II and III as compared with wing I is attributed to their planform area distribution relative to the moment reference center. The slight zero shift of curves is the result of tunnel flow angularity.

The most pronounced effects due to leading-edge curvature and decreasing spanwise leading-edge radius were on the drag characteristics. As indicated in figures 3(b) and 4, the changes in drag are independent of lift. At M = 3, a 26-percent reduction in zero-lift drag due to combined leading-edge curvature and decreasing spanwise leading-edge radius (wing III compared with wing I) was obtained, the largest part of the reduction, 17 percent, being due to leading-edge curvature alone (wing II compared with wing I). At M = 6, a greater zero-lift drag reduction of 50 percent is noted, the largest part of the reduction, 29 percent, resulting from decreasing spanwise leading-edge radius.

The effects of leading-edge curvature and decreasing spanwise leading-edge radius on the lift-drag ratios are presented in figure 5. The aforementioned reductions in zero-lift drag, as a result of leading-edge modifications, are reflected as increases in lift-drag ratios. These combined leading-edge modifications resulted in a 16- and 32-percent increase in maximum lift-drag ratio at M = 3 and 6, respectively, with a slight decrease in lift coefficient for maximum lift-drag ratio.

6

CONCLUSIONS

Results of force tests of three slab-sided delta planform wings, one with a straight leading edge and two with curved leading edges, at Mach numbers of 3 and 6 are as follows:

1. The lift and pitching-moment characteristics of both curved leading-edge wings were essentially identical to those of the straight leading-edge wing.

2. Zero-lift drag coefficients of the curved leading-edge wing with spanwise decreasing leading-edge radius and corresponding wing thickness were 26 and 50 percent lower at Mach numbers of 3 and 6, respectively, than those for the straight leading-edge wing.

3. The curved leading-edge wing with constant spanwise leading-edge radius and wing thickness indicated that approximately one-half of the zero-lift drag-coefficient reduction due to leading-edge curvature with decreasing leading-edge radius and corresponding wing thickness was the result of leading-edge curvature, the remaining reduction being due to decreasing leading-edge radius with corresponding decreasing wing thickness.

4. Maximum lift-drag ratios 16 and 32 percent higher than those for the straight leading-edge wing, at Mach numbers of 3 and 6, respectively, were noted for the curved leading-edge wing with decreasing spanwise leading-edge radius and wing thickness.

Langley Research Center,
    National Aeronautics and Space Administration,
        Langley Station, Hampton, Va., June 19, 1964.

APPENDIX A

A METHOD OF INTRODUCING CURVATURE TO A BLUNT HIGH-SPEED

AERODYNAMIC LEADING EDGE

As noted in reference 5, based on the theoretical and experimental results of references 6 and 7, the laminar convective heating rate $\frac{dH}{dt}$ of an aerodynamic leading edge at high-speed flights is a function of leading-edge geometry and is expressed approximately as

$$\frac{dH}{dt} \approx \frac{\cos \Lambda}{\sqrt{R}}$$

From this expression it is noted that by introducing curvature to a leading edge such that its sweep is continuously increased over the leading-edge span, a corresponding reduction in leading-edge radius could be made without altering the geometric relationship on the right-hand side of the equation.

To introduce curvature to a straight leading-edge surface such that the geometric relationship of the leading edge associated with laminar convective heating is not altered, requires that

$$\frac{\cos \Lambda}{\sqrt{R}} = \frac{\cos \Lambda'}{\sqrt{R'}} \tag{A1}$$

To include aerodynamic surfaces at angles of attack other than zero, the geometric sweep angle is replaced by the effective sweep angle which is defined by

$$\cos \Lambda_e = \sqrt{1 - (\cos \alpha \sin \Lambda)^2} \tag{A2}$$

and

$$\cos \Lambda_e' = \sqrt{1 - (\cos \alpha \sin \Lambda')^2} \tag{A3}$$

Therefore, changing the geometric sweep angle in equation (A1) to the effective sweep angle by using equations (A2) and (A3) yields

$$\frac{\sqrt{1 - (\cos \alpha \sin \Lambda)^2}}{\sqrt{R}} = \frac{\sqrt{1 - (\cos \alpha \sin \Lambda')^2}}{\sqrt{R'}} \tag{A4}$$

8

By using the simplification that the aerodynamic surface is slab sided and that the curved leading-edge radius R' is equal to the local wing half-thickness t (derivation of the leading-edge radius follows), the geometric relationships of figure 6 shows that

$$t = t_r\left(1 - \frac{x}{A}\right)$$

Letting the root half-thickness of the slab-sided curved leading-edge surface be equal to the half-thickness of the slab-sided straight leading-edge surface and therefore equal to its leading-edge radius, $t_r = R$, and thus

$$R' \approx t = R\left(1 - \frac{x}{A}\right)$$

Substituting this expression into equation (A4) for R' yields

$$\sqrt{1 - (\cos \alpha \sin \Lambda)^2} = \frac{\sqrt{1 - (\cos \alpha \sin \Lambda')^2}}{\sqrt{1 - \frac{x}{A}}}$$

Solving this equation for $\sin \Lambda'$ and expressing the results in terms of $\tan \Lambda'$, which is the local slope of the curved leading edge, gives

$$\tan \Lambda' = -\frac{dy}{dx} = \frac{\sqrt{1 - \cos^2\Lambda_e\left(1 - \frac{x}{A}\right)}}{\sqrt{\cos^2\alpha - 1 + \cos^2\Lambda_e\left(1 - \frac{x}{A}\right)}} \tag{A5}$$

Integration of equation (A5) gives

$$y = \sqrt{\frac{A}{\cos^2\Lambda_e} - A + x}\sqrt{\frac{A\cos^2\alpha}{\cos^2\Lambda_e} - \frac{A}{\cos^2\Lambda_e} + A - x}$$

$$+ \frac{A\cos^2\alpha}{\cos^2\Lambda_e} \sin^{-1}\frac{\sqrt{\frac{A\cos^2\alpha}{\cos^2\Lambda_e} - \frac{A}{\cos^2\Lambda_e} + A - x}}{\sqrt{\frac{A\cos^2\alpha}{\cos^2\Lambda_e}}} + B \tag{A6}$$

which is the equation of the curved leading edge. The values of the constant A and the constant of integration B are determined by boundary conditions at the tip of the curved leading-edge surface. From equation (A5) the value of A is determined by choosing values of Λ' and x at the tip of the curved wing and using known values of the straight leading-edge surface which defines Λ_e and α. With A determined, the value of B is calculated from equation (A6) by letting $y = 0$ when x is the span of the curved leading-edge surface.

To obtain the leading-edge radius, the geometric relations of figure 6 give

$$\frac{D + G}{H - F} = \frac{E}{H} \quad \text{or} \quad D = E - \frac{EF}{H} - G$$

but

$$\frac{G}{R'} = \frac{t_r}{H} \quad \text{or} \quad G = \frac{R' t_r}{H}$$

so

$$D = E - \frac{EF}{H} - \frac{R' t_r}{H}$$

but

$$D = C - R'$$

so

$$C - R' = E - \frac{EF}{H} - \frac{R' t_r}{H}$$

or

$$\frac{EF}{H} - R' + \frac{R' t_r}{H} = E - C$$

where

$$F = \frac{ER'}{t_r}$$

therefore

$$\frac{E^2 R'}{H t_r} - R' + \frac{R' t_r}{H} = E - C$$

and solving for R' yields

$$R' = \frac{C - E}{1 - \dfrac{E^2}{H t_r} - \dfrac{t_r}{H}}$$

where

$$C = \frac{x}{\sin \Lambda'}$$

$$E = \frac{A}{\sin \Lambda'}$$

$$H = \sqrt{t_r^2 + E^2} = \sqrt{t_r^2 + \frac{A^2}{\sin^2 \Lambda'}}$$

therefore

$$R' = \frac{x - A}{\sin \Lambda' - \dfrac{A^2}{t_r \sqrt{t_r^2 \sin^2 \Lambda' + A^2}} - \dfrac{t_r \sin \Lambda'}{\sqrt{t_r^2 + \dfrac{A^2}{\sin^2 \Lambda'}}}} \qquad (A7)$$
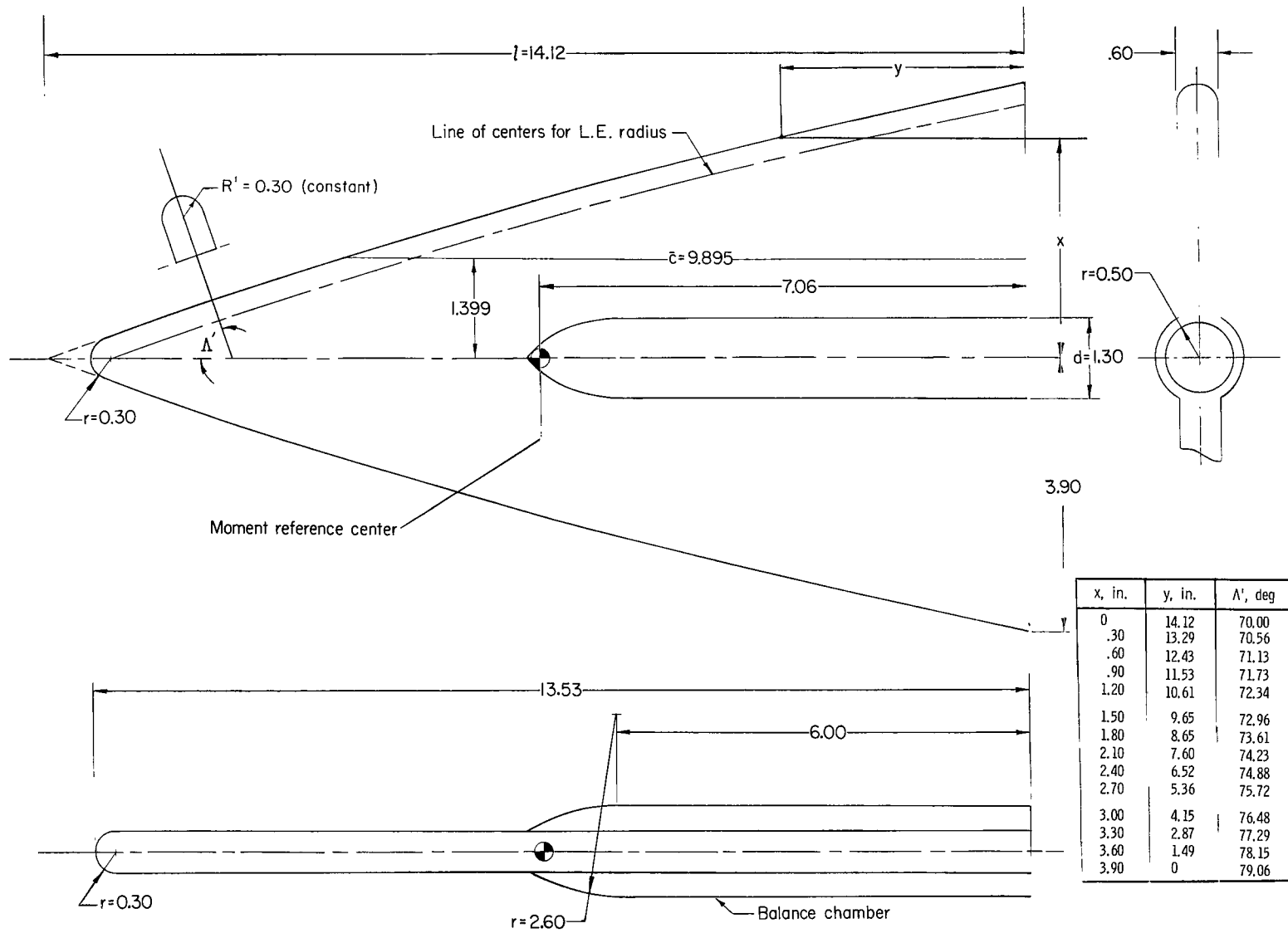
REFERENCES

1. Robinson, Ross B.: Aerodynamic Characteristics at Supersonic Speeds of a Series of Wing-Body Combinations Having Cambered Wings With an Aspect Ratio of 3.5 and a Taper Ratio of 0.2 - Effects of Sweep Angle and Thickness Ratio on the Aerodynamic Characteristics in Pitch at M = 2.01. NACA RM L52E09, 1952.

2. McLellan, Charles H., and Dunning, Robert W.: Factors Affecting the Maximum Lift-Drag Ratio at High Supersonic Speeds. NACA RM L55L20a, 1956.

3. Penland, Jim A.: Aerodynamic Characteristics of a Circular Cylinder at Mach Number 6.86 and Angles of Attack up to 90°. NACA TN 3861, 1957. (Supersedes NACA RM L54A14.)

4. Spencer, Bernard, Jr., and Hammond, Alexander D.: Low-Speed Longitudinal Aerodynamic Characteristics Associated With a Series of Low-Aspect-Ratio Wings Having Variations in Leading-Edge Contour. NASA TN D-1374, 1962.

5. Seiff, Alvin, and Allen, H. Julian: Some Aspects of the Design of Hypersonic Boost-Glide Aircraft. NACA RM A55E26, 1955.

6. Eggers, A. J., Jr., Hansen, C. Frederick, and Cunningham, Bernard E.: Theoretical and Experimental Investigation of the Effect of Yaw on Heat Transfer to Circular Cylinders in Hypersonic Flow. NACA RM A55E02, 1955.

7. Feller, William V.: Investigation of Equilibrium Temperatures and Average Laminar Heat-Transfer Coefficients for the Front Half of Swept Circular Cylinders at a Mach Number of 6.9. NACA RM L55F08a, 1955.

8. Stokes, George M.: Description of a 2-Foot Hypersonic Facility at the Langley Research Center. NASA TN D-939, 1961.
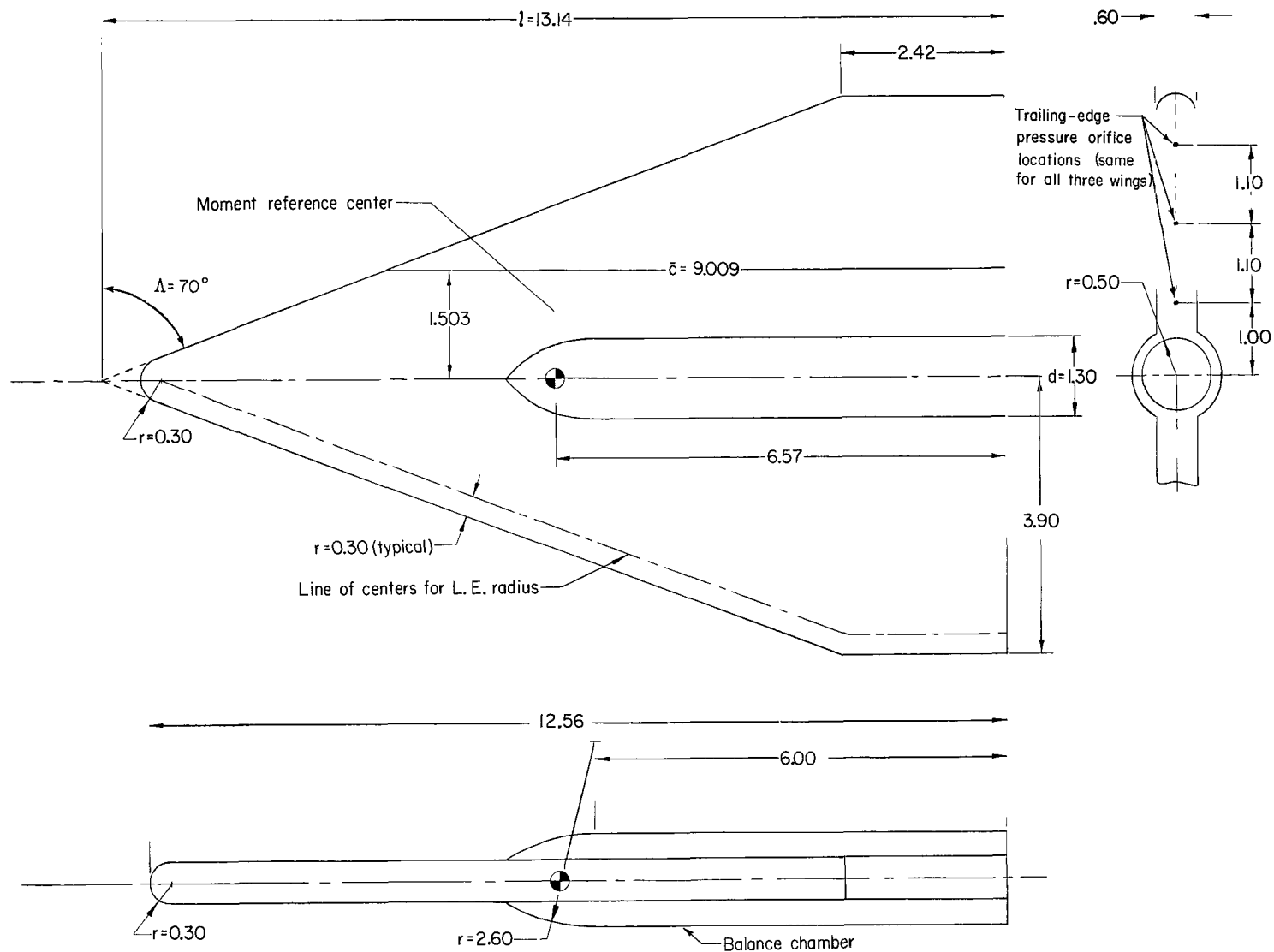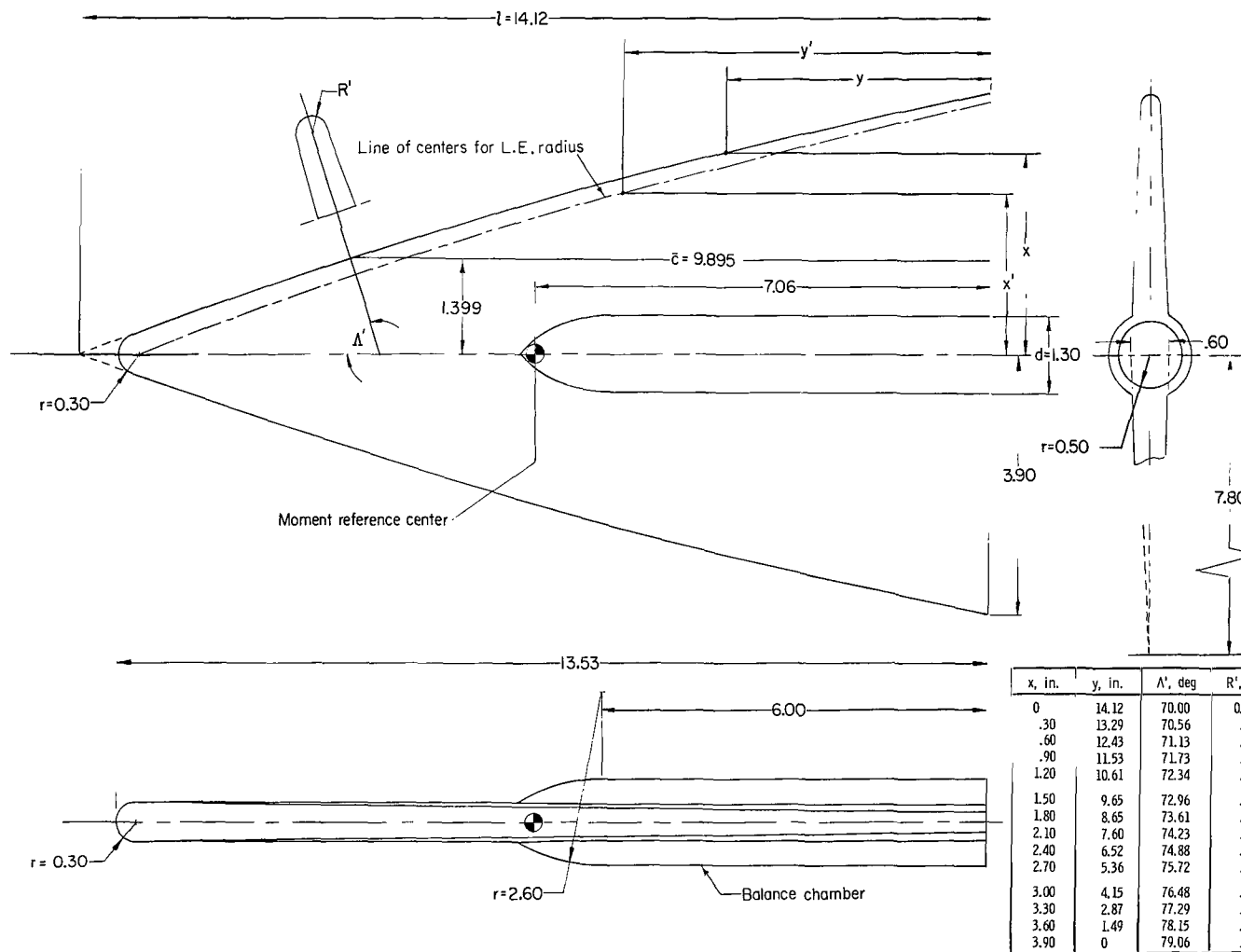
(a) Wing I.

Figure 1.- Dimensional details of wings. All dimensions are in inches unless otherwise noted.
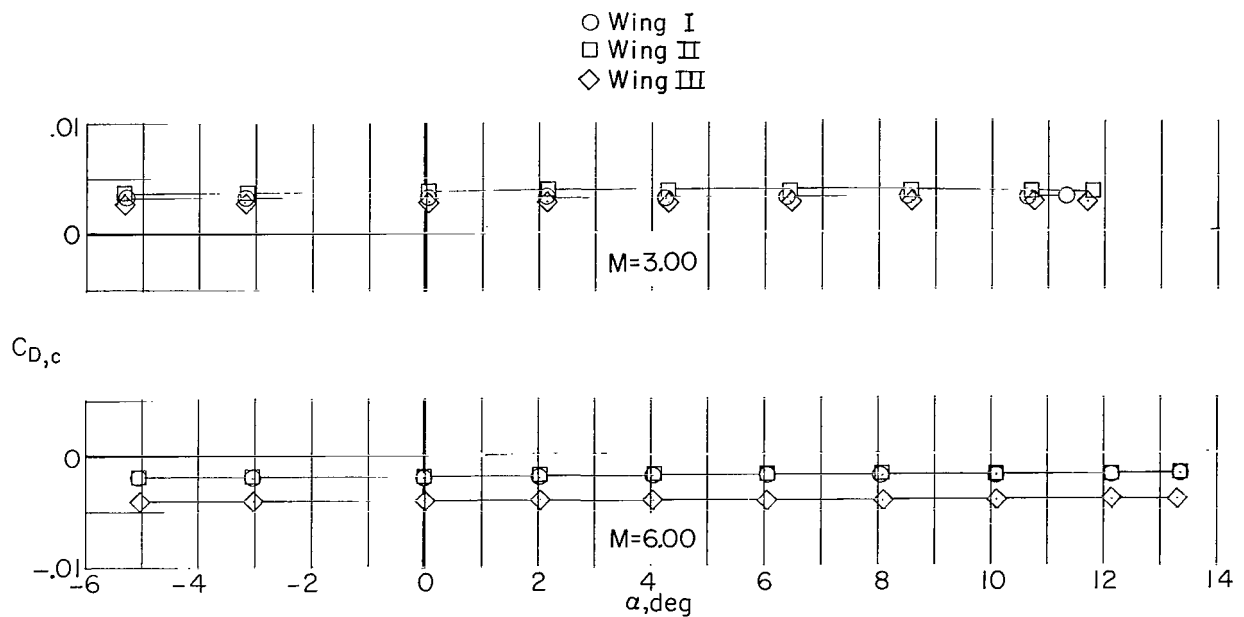
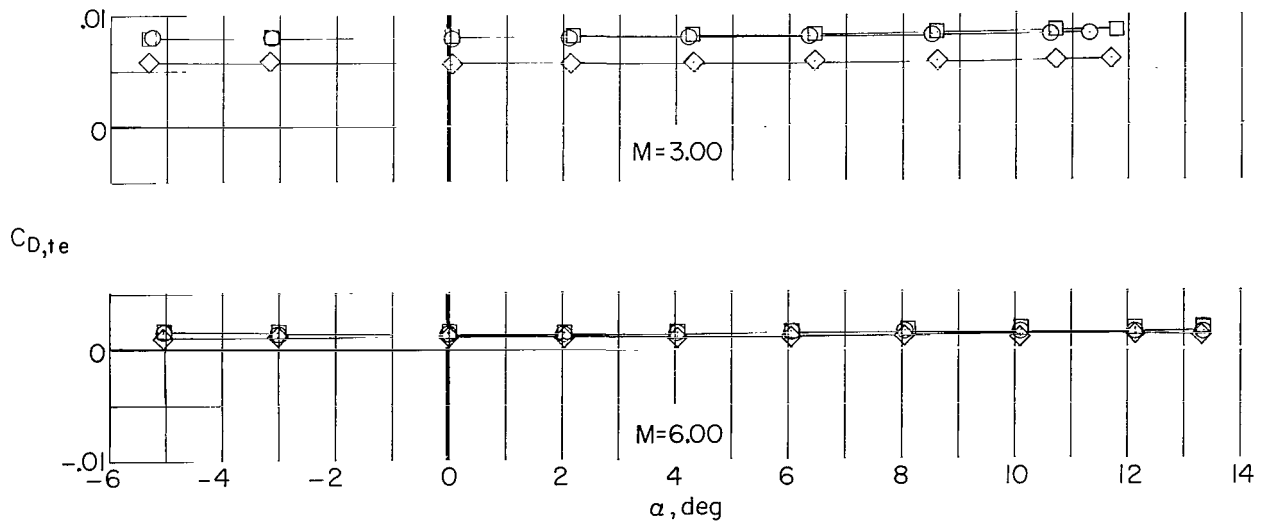| x, in.	y, in.	Λ', deg
0	14.12	70.00
.30	13.29	70.56
.60	12.43	71.13
.90	11.53	71.73
1.20	10.61	72.34
1.50	9.65	72.96
1.80	8.65	73.61
2.10	7.60	74.23
2.40	6.52	74.88
2.70	5.36	75.72
3.00	4.15	76.48
3.30	2.87	77.29
3.60	1.49	78.15
3.90	0	79.06

(b) Wing II.

Figure 1.- Continued.

x, in.	y, in.	Λ', deg	R', in.	x', in.	y', in.
0	14.12	70.00	0.31	0	13.23
.30	13.29	70.56	.30	.33	12.34
.60	12.43	71.13	.29	.64	11.44
.90	11.53	71.73	.28	.95	10.53
1.20	10.61	72.34	.26	1.26	9.58
1.50	9.65	72.96	.25	1.57	8.58
1.80	8.65	73.61	.24	1.88	7.54
2.10	7.60	74.23	.23	2.19	6.46
2.40	6.52	74.88	.22	2.50	5.31
2.70	5.36	75.72	.20	2.81	4.10
3.00	4.15	76.48	.19	3.12	2.84
3.30	2.87	77.29	.18	3.44	1.45
3.60	1.49	78.15	.17	3.75	.03
3.90	0	79.06	.16		

(c) Wing III.

Figure 1.- Concluded.

15

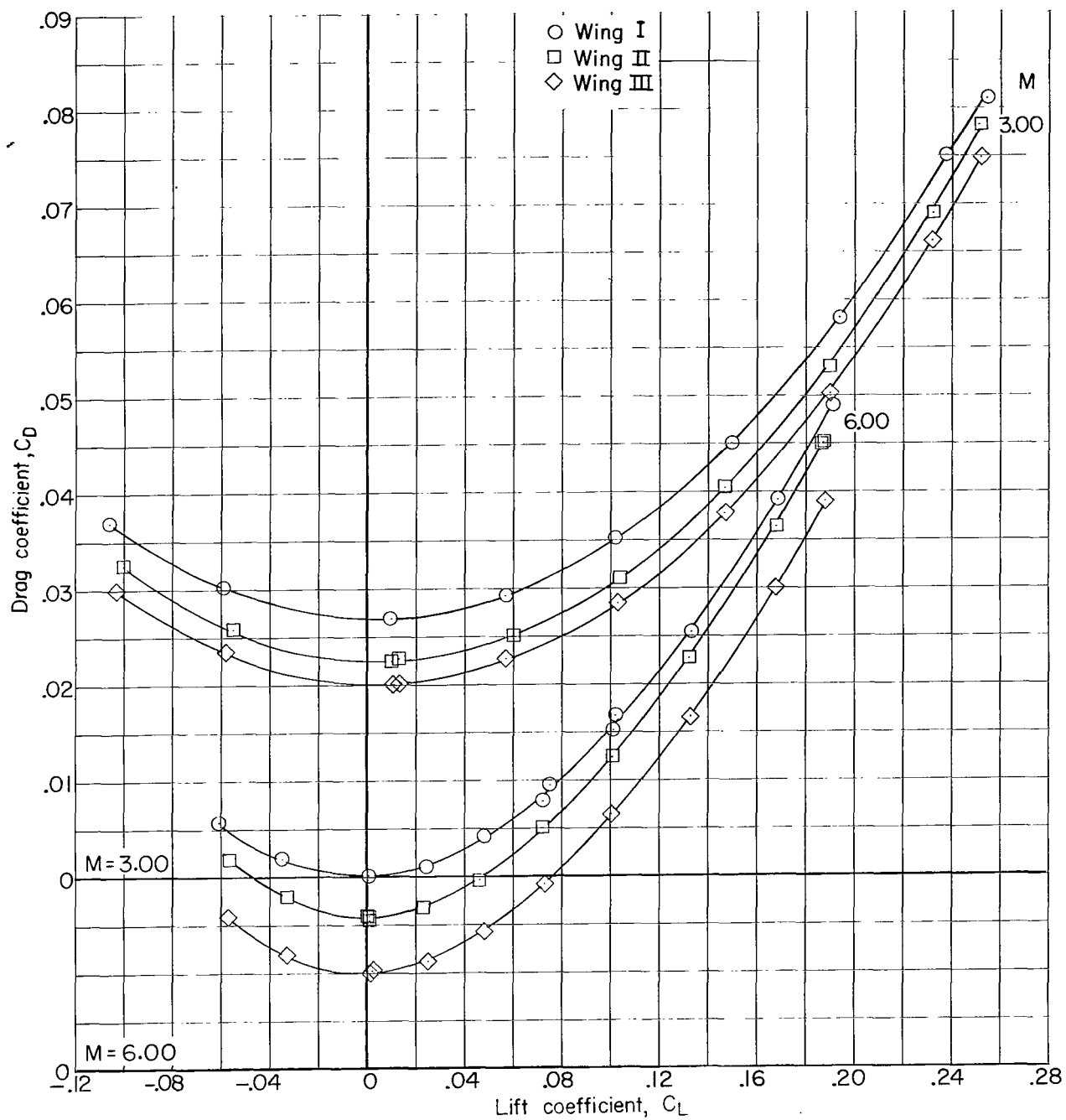(a) Chamber-pressure drag coefficient.

(b) Trailing-edge drag coefficient.

Figure 2.- Variation of chamber-pressure and trailing-edge drag coefficients with angle of attack.
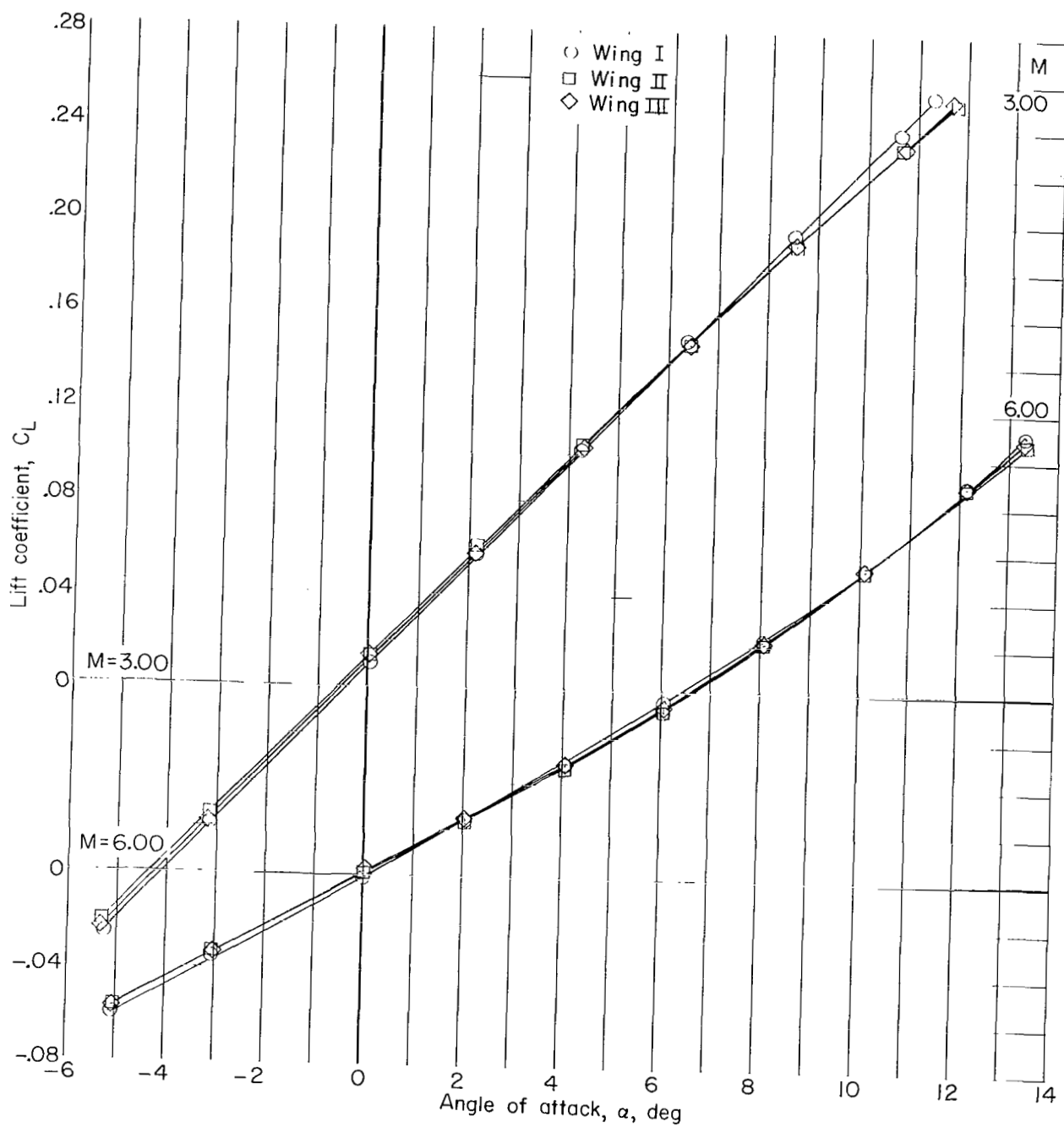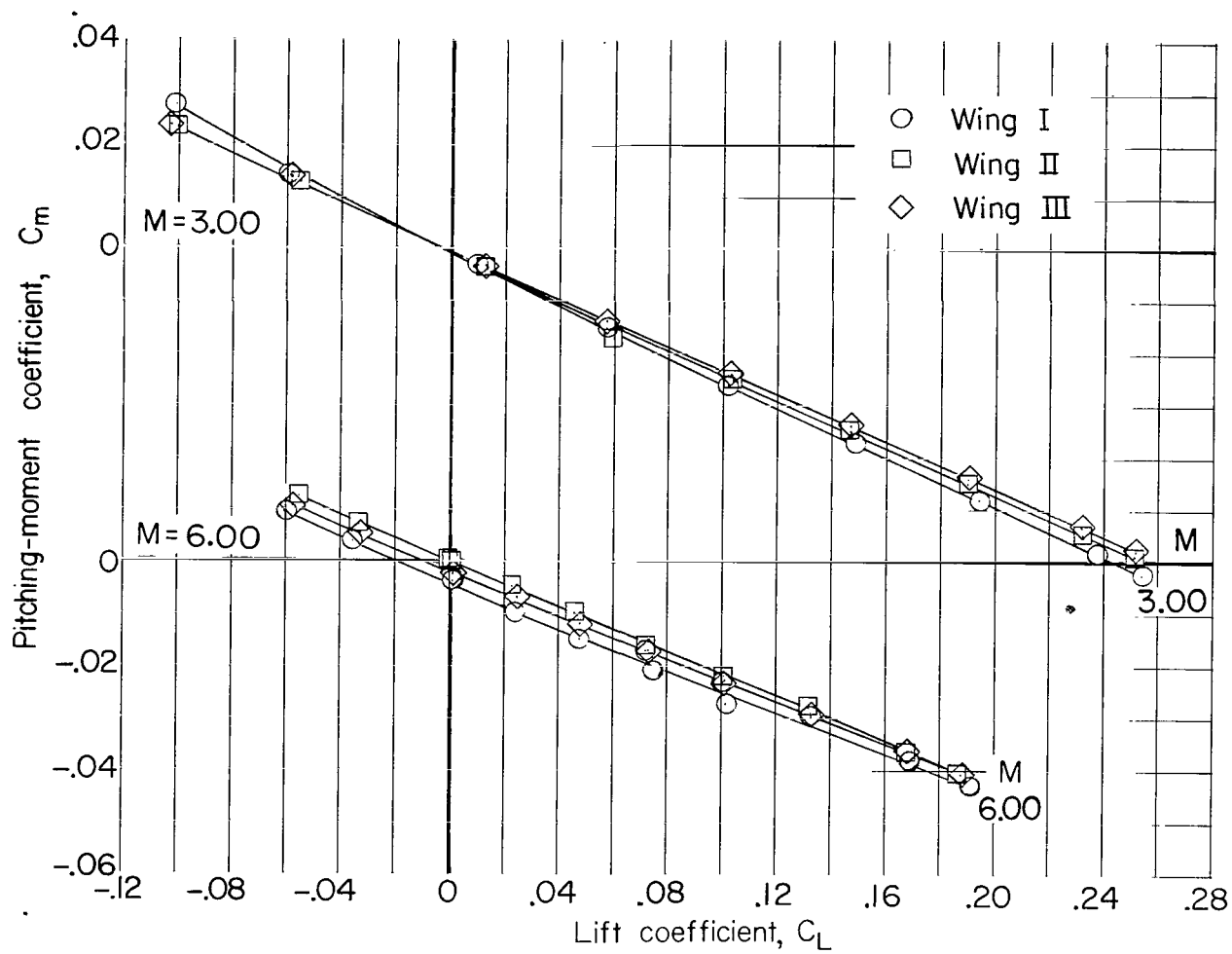
(a) Lift coefficient.

Figure 3.- Static longitudinal aerodynamic characteristics of the three wings at Mach numbers 3.00 and 6.00.

(b) Drag coefficient.

Figure 3.- Continued.

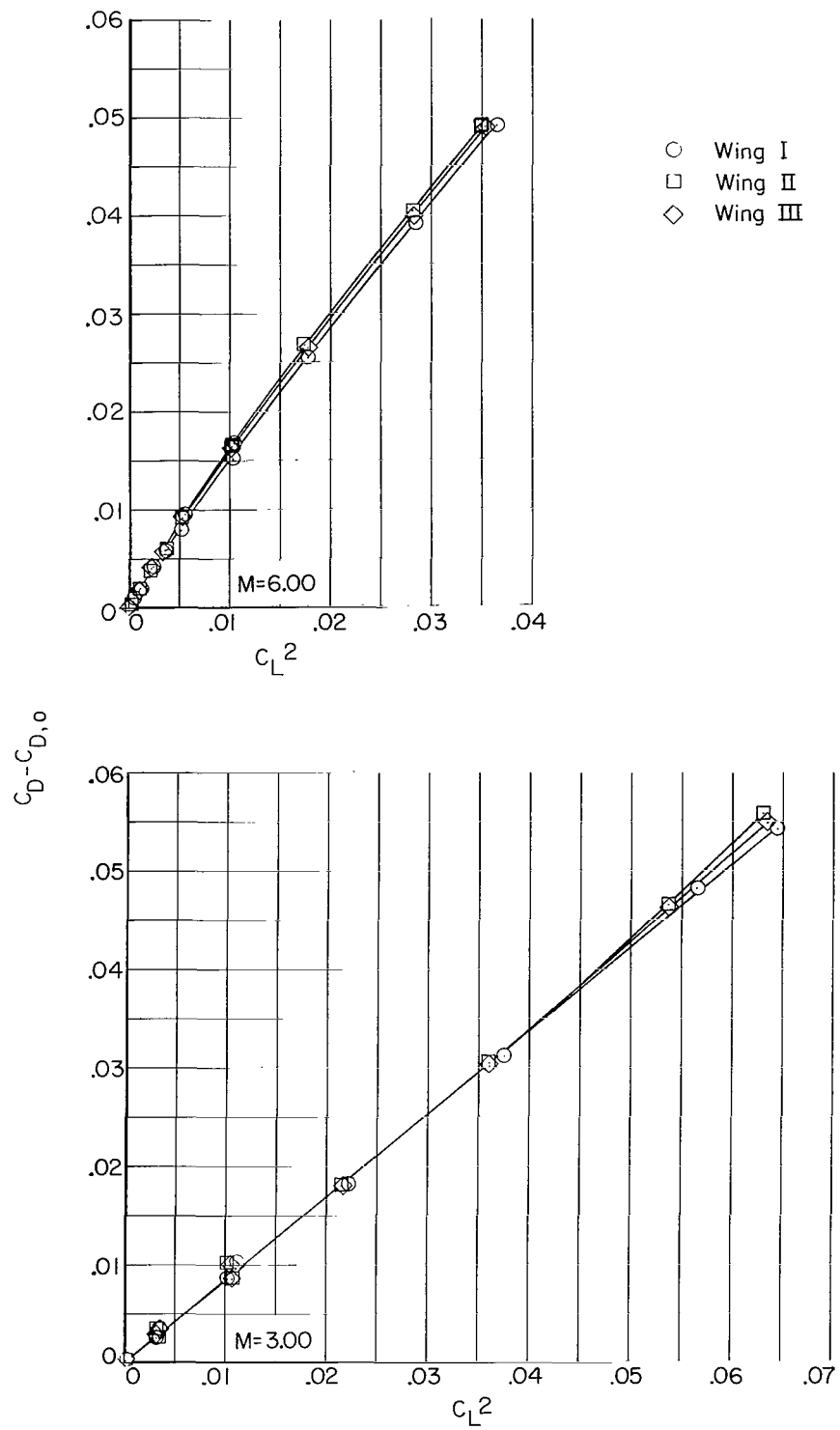(c) Pitching-moment coefficient.

Figure 3.- Concluded.
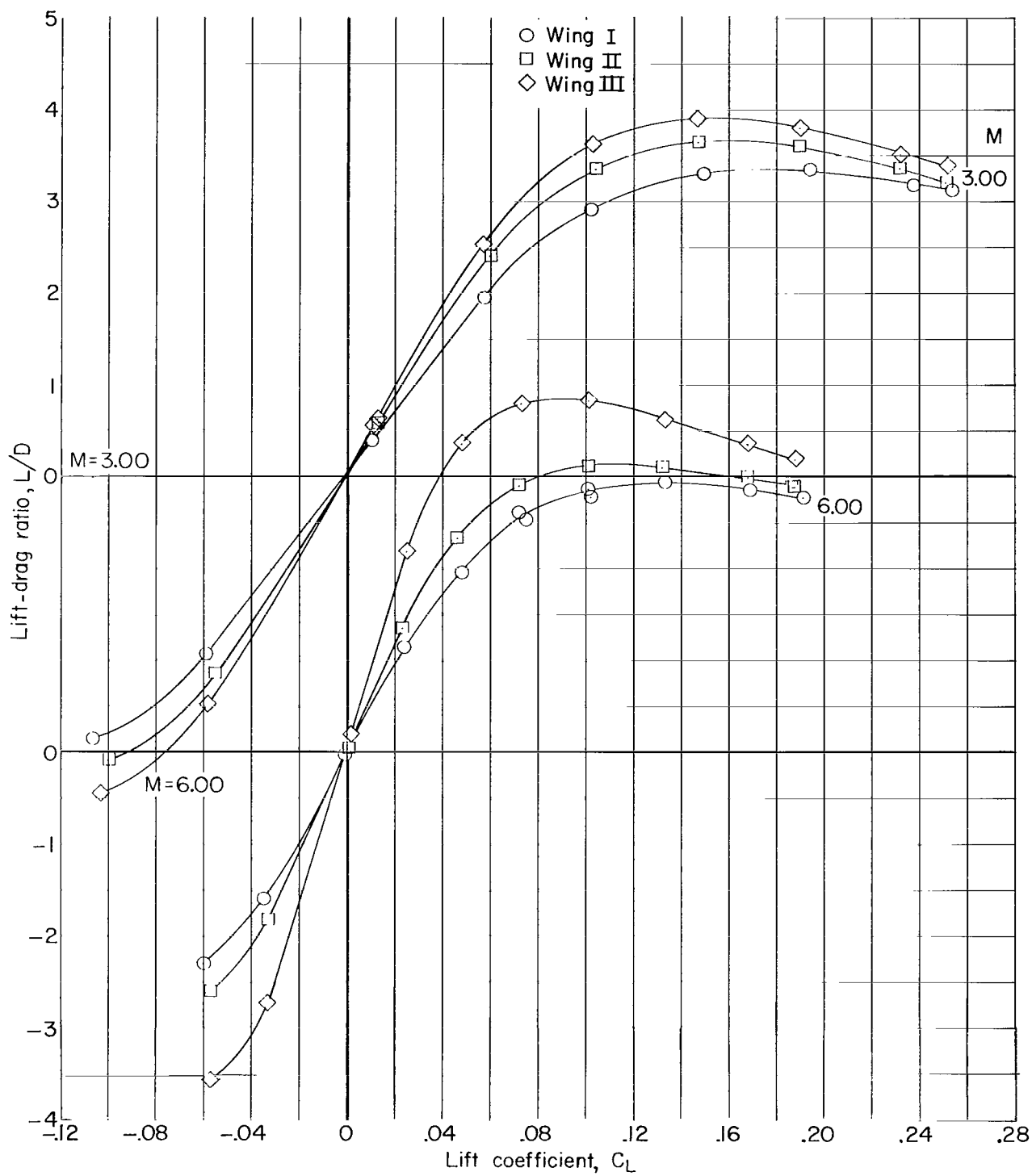
Figure 4.- Drag coefficient increment due to lift.

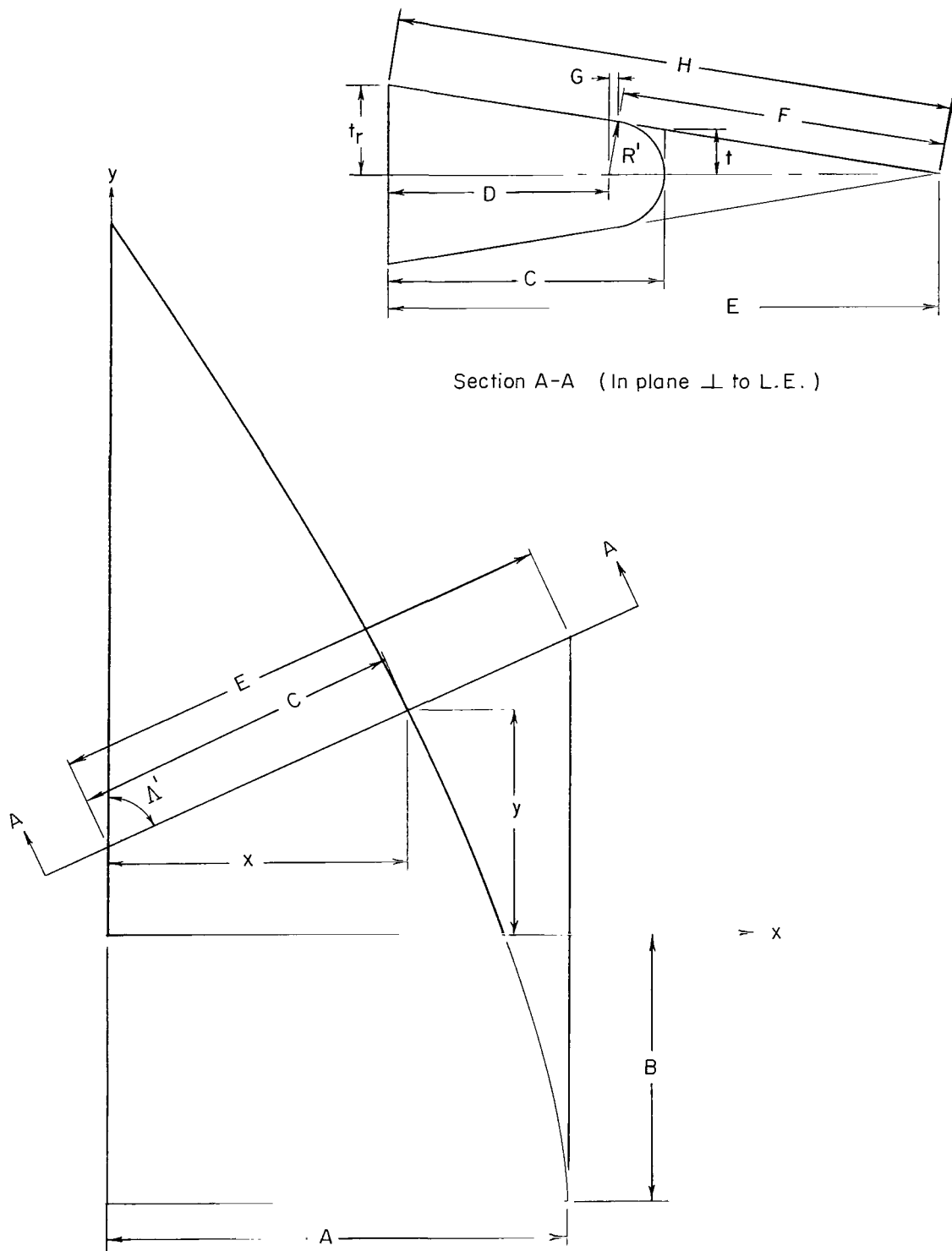Figure 5.- Variation of lift-drag ratio with lift coefficient.

Section A-A   (In plane ⊥ to L.E.)

Figure 6.- Geometric relations for determining the leading-edge curvature and radius.

"The aeronautical and space activities of the United States shall be conducted so as to contribute . . . to the expansion of human knowledge of phenomena in the atmosphere and space. The Administration shall provide for the widest practicable and appropriate dissemination of information concerning its activities and the results thereof."

—NATIONAL AERONAUTICS AND SPACE ACT OF 1958

NASA SCIENTIFIC AND TECHNICAL PUBLICATIONS

TECHNICAL REPORTS: Scientific and technical information considered important, complete, and a lasting contribution to existing knowledge.

TECHNICAL NOTES: Information less broad in scope but nevertheless of importance as a contribution to existing knowledge.

TECHNICAL MEMORANDUMS: Information receiving limited distribution because of preliminary data, security classification, or other reasons.

CONTRACTOR REPORTS: Technical information generated in connection with a NASA contract or grant and released under NASA auspices.

TECHNICAL TRANSLATIONS: Information published in a foreign language considered to merit NASA distribution in English.

TECHNICAL REPRINTS: Information derived from NASA activities and initially published in the form of journal articles.

SPECIAL PUBLICATIONS: Information derived from or of value to NASA activities but not necessarily reporting the results of individual NASA-programmed scientific efforts. Publications include conference proceedings, monographs, data compilations, handbooks, sourcebooks, and special bibliographies.

Details on the availability of these publications may be obtained from:

SCIENTIFIC AND TECHNICAL INFORMATION DIVISION

NATIONAL AERONAUTICS AND SPACE ADMINISTRATION

Washington, D.C. 20546